High Throughput Synthesis of Micellar Nanocomposites via Liquid-Liquid Electrospray

Author: Kil Ho Lee[1]
Advisors: Dr. Jessica Winter[1,2] and Dr. Barbara Wyslouzil[1,3]
William G. Lowrie Department of Chemical and Biomolecular Engineering[1]
Department of Biomedical Engineering[2]
Department of Chemistry and Biochemistry[3]

Introduction

Synthesis methods for micellar nanocomposites have been developed by several research groups, but the standard methods share the common disadvantage of relatively low, laboratory scale production levels.[1-10] As a result, the techniques that could achieve high production level have been developed in more recent years; however, the product quality and the process controllability are still low. Meanwhile, the interest in applications of nanocomposites, especially in biological/biomedical sciences, continues to grow.[8] As a result, developing a high throughput production platform is a critical step to furthering current biomedical strategies. Recently, our research group successfully demonstrated a semi-continuous synthesis route incorporating electrospray techniques that are often used in aerosol science.[11] The purpose of this study is to develop a novel synthesis route for micellar nanocomposites, or micelles, using Liquid-Liquid Electrospray (LLE) in a surfactant free environment. This study will establish a semi-continuous platform to generate high quality nanocomposites at a large scale for a number of biological applications, including bio-imaging, cell separation, and drug delivery. Specifically, the aims of this work are to:

Aim 1: Develop a liquid-liquid electrospray configuration for high throughput synthesis.

Aim 2: Identify the parameters suitable to achieve stable, surfactant free synthesis via LLE.

Aim 3: Evaluate the uniformity and functionality of nanocomposites synthesized via LLE.

Aim 4: Propose the next generation micellar electrospray configuration using a membrane filter to further scale up and optimize the process.

Multimodal Nanocomposites

Nanocomposites are materials that incorporate multiple phases on a nanometer scale that retain component specific functionality and properties. For example, polymeric micellar nanocomposites, or micelles, are widely studied nanocomposites. Micelle structure is derived from the amphiphilic block copolymer (BCP) chains that self assemble to form a hydrophobic core region surrounded by a hydrophilic corona. Most biological applications of micelles utilize the hydrophobic core to encapsulate a variety of hydrophobic materials including nanoparticles (NPs) and drug molecules.[12] Given their unique structural properties, micelles and other multimodal nanocomposites that integrate two or more types of NPs/molecules have gained significant attention in the biomedical science and engineering.[13-18] As illustrated in Figure 1, several research groups have demonstrated the use of polymeric colloids encapsulating quantum dots for bio-imaging. Quantum Dots (QDs) are fluorescent semiconducting NPs that emit fluorescent light with narrow emission spectra. Dubertret et al. demonstrated the synthesis of lipid-*poly*(*ethylene glycol*) amphiphiles to create micelles encapsulating a single QD. By employing surface modification techniques, DNA conjugated QD-micelles were used for *in vivo* imaging of *Xenopus* embryos.[19] Another example of polymeric colloids encapsulating QDs, shown by Gao et al., utilized the hydrophobic interactions between the hydrophobic block of triblock amphiphilic polymer and the surface ligand of QDs, tri-*n*-octylphosphoine oxide (TOPO), to generate polymeric colloids.[20] Furthermore, Han et al. demonstrated the use of multiple quantum dots emitting different wavelength of fluorescent signals encapsulated in solid polymeric microbeads to enable multiplexing. Here, the size of microbeads was around 1.2 μm in diameter.[21] However, the idea of

individual microbeads exhibiting multiple fluorescent signatures demonstrated the benefits of multimodal composites.

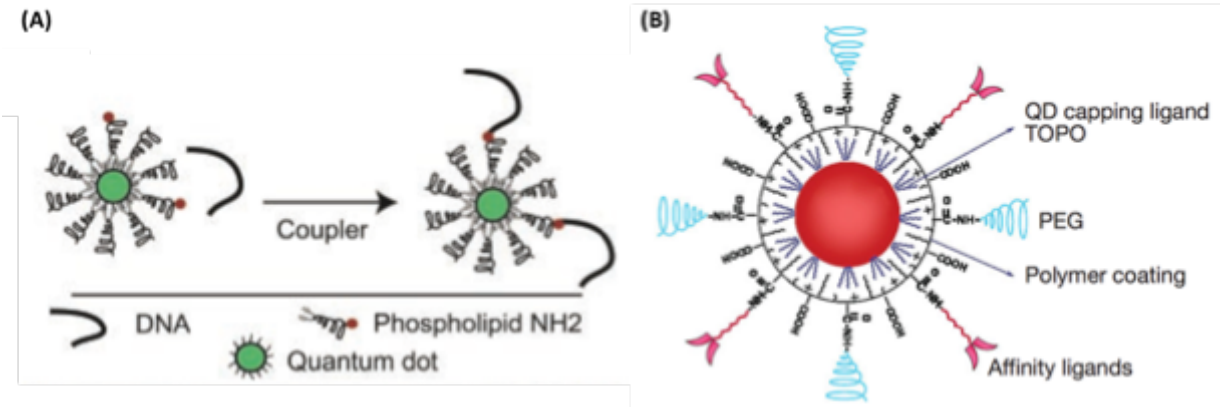

Figure 1. Nanocomposites encapsulating QDs: (**A**) phospholipid polymeric amphiphiles surrounding QDs.[19] (**B**) triblock copolymer consisting polybutylacrylate, polyehtylacrylate, and polymethacrylic acid segments interacting with TOPO, forming polymeric colloid.[20]

As an alternative to polymeric composites, other studies have developed silica composites encapsulating magnetic materials such as superparamagnetic iron oxide NPs (SPIONs).[22] Also, micellar nanocomposites encapsulating both magnetic and fluorescent NPs (QDs) have been successfully synthesized to provide dual functionalities.[2,3]

The unique properties of NPs provide the opportunity to enhance the current biomedical strategies. However, the primary challenge is that the synthesis approaches yielding the most monodispersed, and the highest quality NPs are done in organic environment. Hence, the NPs are hydrophobic in nature. As a result, for biological applications, the ability to transfer the organic NPs into aqueous system is required. Our research efforts have focused on synthesizing micellar nanocomposites encapsulating both QDs and SPIONs that could effectively introduce the NPs into aqueous environment packaged inside the micellar sturcutre.[4-7] Figure 2 shows the different types of nanocomposites characterized in our previous work: MultiDots (micelles encapsulating QDs), SuperMags (micelles encapsulating SPIONs), and MagDots (micelles encapsulating both QDs and

SPIONs). These nanocomposites were developed primarily using poly(styrene)-block-poly(ethylene glycol). Packaging the NPs with unique properties into polymeric composites enables simultaneous bio-imaging and cell separation/manipulation. Also, as briefly illustrated above, the functional groups of the hydrophilic corona of the micelles can be conjugated with bio-markers (i.e. DNA or antibody) to target specific cells of interest.

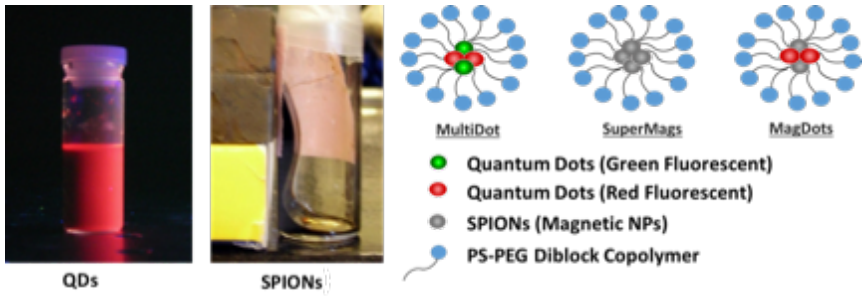

Figure 2. Schematics of different types of nanocomposites developed in Winter group

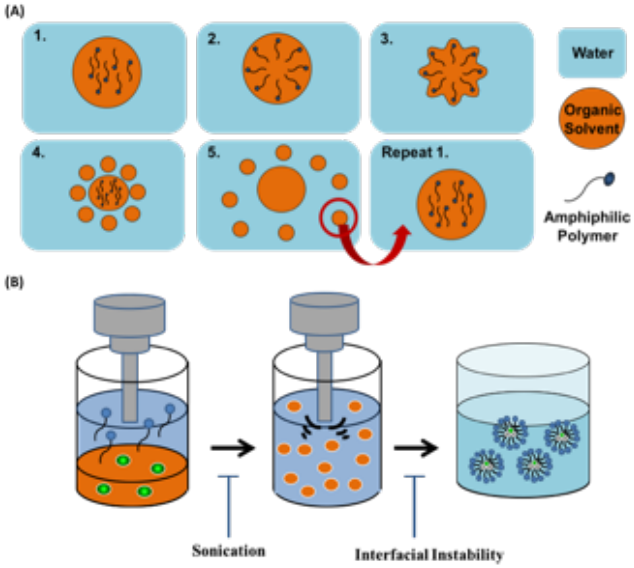

Figure 3. (**A**) Interfacial Instability (IS) process:
1. emulsion droplets form, 2. hydrophilic heads of BCP chains adhere to the water/oil interface,
3. surface tension drops at the interface, 4. ejection of smaller emulsion droplets, 5. daughter droplets repeating IS process. (**B**) Schematic of probe sonication method

Standard Synthesis Methods

Standard synthesis methods for micellar nanocomposites include emulsion based methods[23,24], encapsulation during nucleation[2,22], and self-assembly[1,5,25]. These methods utilize techniques such as dialysis, sonication, and film hydration. Self-assembly is a bottom-up approach that produces the most monodisperse products because the process is largely thermodynamically driven.

Interfacial instability (IS), shown in Figure 3(A), was developed by the Hayward group and utilizes self-assembly of BCP to generate micelles. In IS, an organic solvent comprised of BCP and hydrophobic encapsulants (i.e. NPs) is emulsified in an aqueous solvent.[10] The emulsification results in the formation of emulsion droplets stabilized by the surfactants added in the aqueous phase in most emulsion based synthesis methods. As the emulsion droplets undergo the sudden reduction in surface tension because of the hydrophilic block moving toward the organic/aqueous interface, smaller droplets get ejected.[10,26] In addition, the volatile organic solvent evaporates quickly, increasing the concentration of polymer chains in organic droplets. This process of smaller droplet formation and solvent evaporation repeats itself until the critical micelle concentration (CMC) is reached to promote nanocomposites self-assembly. The first step of IS involves the emulsification of organic solvent; in order to produce monodispersed micelles, uniformly emulsifying the dispersed phase is important. However, this method is limited to a small scale production because of both energy and material transfer limitations during emulsion formation. For example, Figure 3(B) illustrates the use of a probe sonicator, which provides the ultrasonic energy to allow emulsification of two immiscible phases. Here, the intensity of applied energy gradually dissipates as a function of radial distance away from the probe. Hence, scaling up for higher throughput can lead to having not only a large distribution of droplet size, but also to a large dead volume.

Unlike the aforementioned techniques, flash nanoprecipitation (FNP) is a technique that utilizes rapid mixing of solvents for BCP and nanoparticle nucleation. FNP was first developed by Johnson and Prud'homme in 2003, and the initial design incorporated an impinging jets mixer. In FNP, water-miscible solvents such as Tetrahydrofuran (THF) can be used as the organic-rich stream dissolving BCP and organic actives (i.e. NPs).[28] As shown in Figure 4(A), the rapid mixing of

THF and its anti-solvent (i.e. water) via a confined impinging jet mixer (CIJM) promotes the nucleation of BCP. As a result, the nucleation of BCP in the presence of the hydrophobic NPs This study suggests that the mixing time, τ_{mix}, needs to be shorter than the formation time, τ_{flash}.[27,28] Therefore, the use of a jet mixer is crucial to homogenize streams of both solvents on the scale of milliseconds. In addition, studies following the initial FNP design utilized a multi inlet vortex mixer (MIVM), which provided better controllability of operating conditions.[30] Figure 4(B) shows the schematic of FNP operation. FNP has the great advantage of ensuring organic actives being encapsulated in micelles. However, the downside of this process is that the flow rates requirement are significant. For example, in the case of CIJM, the flow rates required range from 3 to 120 mL/min.[31] Therefore, controlled production of high value, low volume products might not be possible via FNP. So far, the methods discussed above have disadvantages in producing high quality nanocomposites with the capability of tunable operation. As a result, it is desired to establish a scalable and tunable synthesis route with the ability to consistently make emulsion droplets. In other words, a novel synthesis platform that incorporates both top-down and bottom-up approaches would overcome the problems associated with the standard techniques.

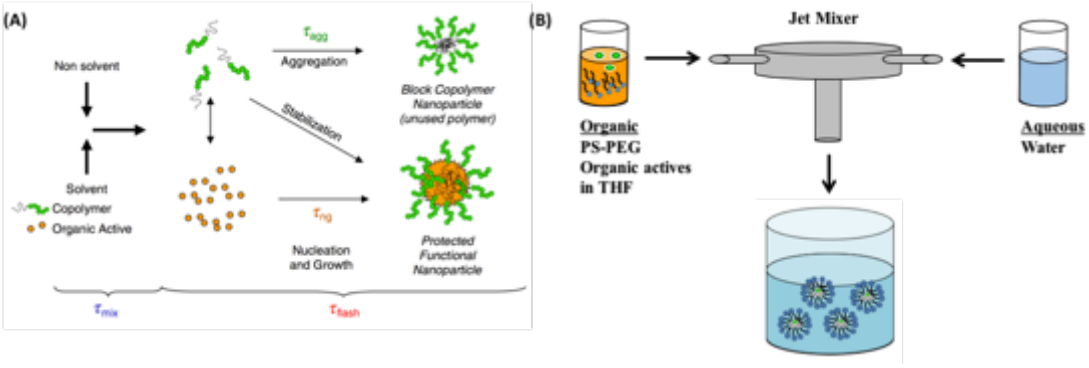

Figure 4. (A) FNP mechanisms: shorter τ_{mix} relative to τ_{flash} promotes nucleation and growth, producing nanocomposites.[27] (B) schematic of FNP with jet mixer (i.e. CIJM or MIVM) rapidly homogenizing solvents.

Electrospray

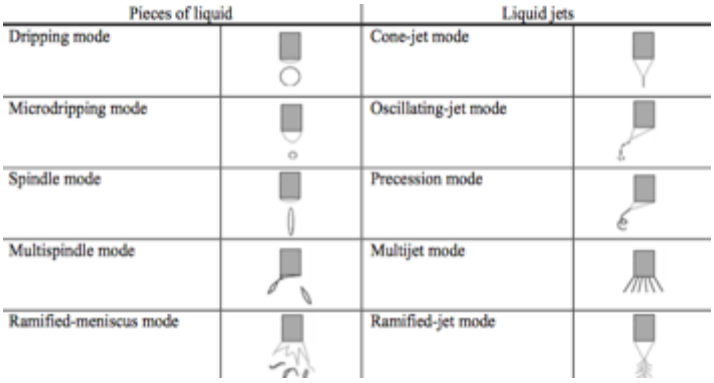

Figure 5. Schematic of various electrospray configurations.[35]

Electrohydrodynamic atomization (EHDA) is a technique widely used in aerosol science that atomizes moving fluids by electrical forces.[32] The concept was first demonstrated by Zeleny in 1917. In that study, ethanol flowed through a tube with diameter slightly less than 1 mm, while a voltage was applied to the fluid in motion. In a particular voltage range, the electrified liquid can form a conical shape at the tip of the capillary from which a jet is ejected that then breaks up into droplets.[35] Taylor explained the deformation of the fluid in an electrical field that forms a conical shape jet.[34] Additional studies have identified various modes of electrospray processes. Figure 5 shows the classification of the modes of electrospray, which includes the conical liquid jet, or cone-jet mode. The parameters that drive these different spray characteristics include (1) fluid viscosity, (2) applied voltage, and (3) dimensions of capillary.[35]

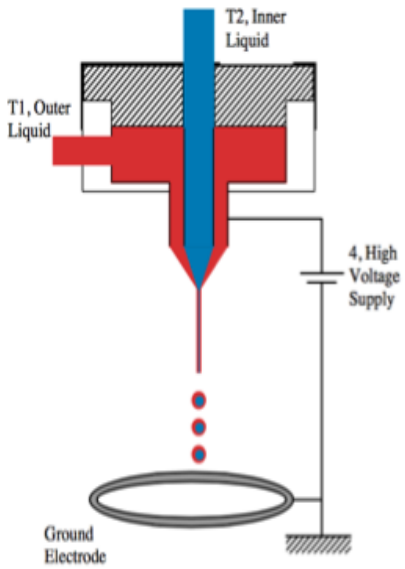

Figure 6. Schematic of coaxial electrospray configuration.[38]

More recent studies report the use of coaxial electrospray, which consists of nested, concentric needles to process two different liquids through the capillary.[36] Loscertales *et al*. described the use of coaxial electrospray to generate monodispersed emulsion droplets on the nanometer scale. Here, two immiscible liquids flow through the inner and outer needle, as shown in Figure 5. The high voltage supply

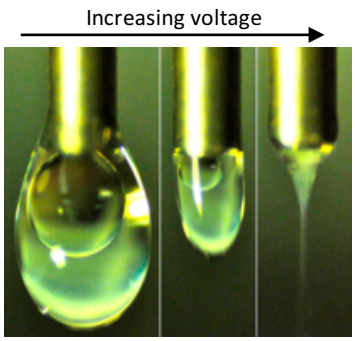

Figure 7. Coaxial electrospray: spraying BCP/NPs suspended chloroform in a conde-jet mode by increasing voltage.[11]

is connected to the outer needle and an electrical potential is generated between the tip of the needle and the grounded electrode. At certain rage of flow rates and the electrical potential in the order of several kilovolts, a cone-jet mode can be established at the exit of needles. Using the coaxial electrospray, this study demonstrated the compound jet capable of generating water-in-oil emulsion droplets. These droplets consist of two immiscible phases flowing through inner and outer needle. Specifically, water flowing through the inner needle formed a Taylor cone inside of olive oil flowing through the annular gap between the two needles.[36] Followed by Loscertale's work, the ability to spray a liquid conductor surrounded by a liquid insulator to form micro-emulstion droplets have been utilized for a variety of applications. For example, the coaxial electrospray configurations was used to synthesize a number of micro/nanoscale products such as microbubbles, fibers, lipoplex nanoparticles, and plasmid DNA/PEI popyplexes.[37,38]

More recent advancement of coaxial electrospray technique demonstrated a Tylor cone of an insulating fluid surrounded by a conducting fluid. Duong *et al*. developed the electrospray configuration, called Aero-IS, to produce micellar nanocomposites encapsulating NPs (i.e. QDs and SPIONs), using a coaxial electrospray to generate an emulsion that then underwent IS.[11] The intent of this study was to develop a stable coaxial electrospray configuration to spray dielectric organic solvent in a cone-jet mode. Poly(styrene-b-ethylene oxide), or PS-PEO (PS 9.5 kDa:PEO 18.0 kDa), was the BCP used to form micellar structure. Along with BCP, hydrophobic SPIONs and QDs were suspended in chloroform ($CHCl_3$ electrical conductivity: ~ 2 x 10^{-6} S/m).[39] This

polymer and NPs suspended in solvent were processed in the inner needle. The outer needle was used to process 5% w/v Poly(vinyl alcohol), or PVA, solution. Figure 6 shows how the spraying mode changes from dripping mode to cone-jet mode. Because the two liquids are immiscible, the organic droplet inside of the aqueous droplet is clearly visible in the dripping mode. A voltage difference of ~ 3.5kV was sufficient to deform the streams and spray compound droplets from the cone-jet. These droplets were collected in a dish containing a water reservoir. Chloroform evaporation then promoted IS to synthesize MultiDots, SuperMags, and MagDots.[11] The aforementioned electrospray techniques enable a single step emulsion formation, and suggests the flexibility to accomplish a wide range of emulsion synthesis and applications. In comparison to FNP, Aero-IS has the ability to process smaller volumes of fluids; hence, it provides the ability to generate high value products in a controlled manner.

Liquid-Liquid Electrospray (LLE)

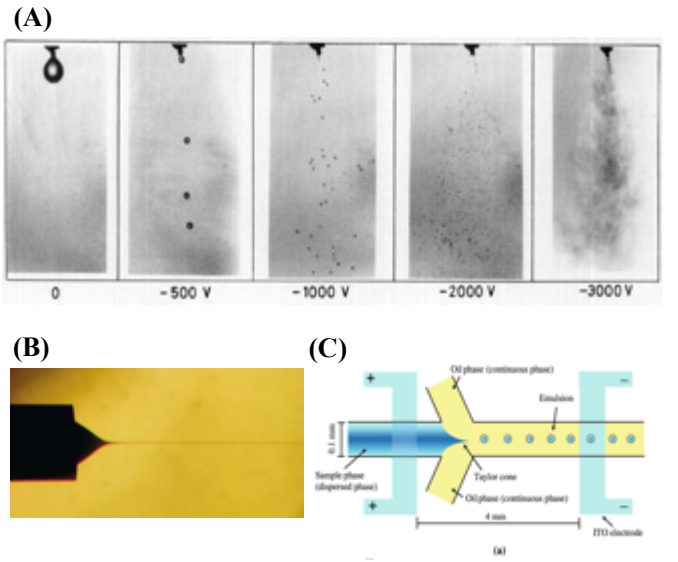

Figure 8. (**A**) Spraying carbon tetrachloride in distilled water,[40] (**B**) Spraying glycerin in hexane in cone-jet mode,[41] (**C**) Cone-jet mode of spraying aqueous (conductive) phase in oil (nonconductive) phase in the electrospray-coupled microfluidic devices.[42]

Traditional electrospray generates aerosols and oil/water emulsions, as illustrated in the previous section. Stable atomization in a liquid-gas system requires the liquid have some conductivity, and a surfactant may be needed to reduce the surface tension of the liquid so that it can more easily deform and disperse.[40] Based on the same concept, modified electrospray emulsification

techniques have been demonstrated by several research groups. For example, EDHA of liquid in another liquid is termed liquid-liquid system, or liquid-liquid electrospray (LLE).

In LLE, the electrical conductivity of the two fluids dictates how the dispersion occurs. In the initial study done by Sato *et al*., the dispersed phases were dielectrics, which typically have electrical conductivities (κ) ~ 10^{-12} S/m, whereas the continuous phase (i.e. distilled water) was a highly conductive liquid. Figure 7(A) shows EHDA of carbon tetrachloride (κ: 4.0 x 10^{-14} S/m) in distilled water (κ: 2.2 x 10^{-4} S/m) at various applied voltages. Increasing the voltage resulted in an increased frequency of droplet ejection and a decrease in the size of droplets. At the applied voltage -3000 V and above, a cloud of fine emulsion droplets of dispersed phase was formed; droplets were stable enough to remain as emulsion without the presence of surfactants in the continuous phase. When designing the liquid-liquid electrospray configuration, for spraying a nonconductive liquid into a conductive liquid, the challenge is to establish the electrical field between the capillary processing a nonconductive liquid and the grounded electrode submerged in the conductive liquid. Tsouris *et al*. explained, by encasing the metal capillary in a ceramic insulation tube, equipotential between the metallic capillary and the conductive continuous phase can be avoided.[43] More recent studies reported achievement of the cone-jet mode in LLE when a conductive liquid is dispersed in a nonconductive liquid. In one study, glycerin (κ: 2.87 x 10^{-6} S/m) was sprayed in hexane, which is a dielectric.[41] The result is shown in Figure 7(B), which exhibits a stable cone-jet dispersing glycerin. Cone-jet LLE was also demonstrated in Figure 7(C) showing a conductive aqueous liquid sprayed into a nonconductive liquid using an electrospray-coupled microfluidic device; more specifically, 1% w/w poly(lactic-co-glycolic acid), or PLGA, in D.I. water mixed with dimethyl sulfoxide (κ: 2.4 x 10^{-6} S/m) was dispersed in mineral oil with a surfactant (κ: 1.6 x 10^{-7} S/m) by applying high voltage. In these examples, spraying a conductive dispersed phase into an insulating,

or nonconductive, continuous phase permitted achievement of cone-jet mode similar to that observed in Aero-IS. Examples of products synthesized via LLE include nano-silica particles and PLGA microparticles.[42,44,45]

Research Plan

In expanding the application of multimodal nanocomposites, this study will achieve EHDA via LLE by developing a controlled, surfactant free oil/water emulsification process. In this section, the detailed experimental plans for each of the aims, as well as the supporting results from preliminary studies, will be reported.

Aim 1: Develop a liquid-liquid electrospray configuration for high throughput synthesis.

The proposed liquid-liquid electrospray configuration is shown in Figure 8(A). A glass syringe (Hamilton, 1 ml) connected to a stainless steel needle (27 gauge, 410 μm o.d.; 210 μm i.d.) was used to process the chloroform. The needle was insulated using a ceramic thermocouple insulator (793.75 μm o.d.; 508 μm i.d.). The tip of the needle was submerged inside of the Miili-Q water contained in a glass collection vial. The stainless steel wire was insulated using a plastic tubing and placed inside the Milli-Q water in the collection vial. This insulated wire was used as a grounded electrode. As suggested by Tsouris *et al.*, a ceramic insulator incasing the needle was used to avoid equipotential, which hinders the electrical field formation, in the conductive medium as the voltage was applied to the needle. In addition, the glass vial was washed multiple times using a base bath and ultrapure water in order to avoid any debris, or ions that could increase the conductivity of aqueous phase. Lastly, the entire apparatus was placed inside of a plexiglass box in order to maximize the safety of operator handling the metallic equipment exposed to a high electrical current.

The design criteria included the ability to disperse chloroform and to generate stable emulsion droplets. As described in the previous section, a cloud of fine emulsion droplets can be sprayed at a sufficiently high voltage, generating an emulsion that is stable enough to remain in this state without the presence of additional surfactant molecules (i.e., no PVA required). It is important to note that the surfactant molecules used in the emulsion based synthesis methods stabilize emulsion droplets. However, in order to use the final products for biological applications, the downstream purification step is required because the surfactant molecules can be toxic. In addition, removing PVA in the final solution is a challenge due to several technical difficulties.

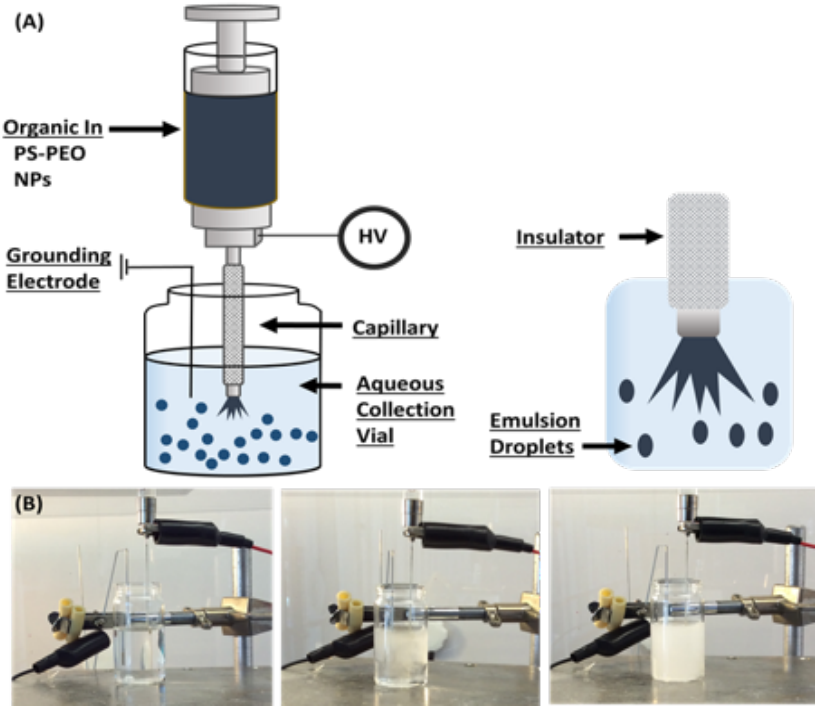

Figure 9. (**A**) Schematic of LLE configuration for nanocomposite synthesis: ceramic insulator incased stainless steel capillary with a high voltage supply attached. (**B**) Chloroform emulsification via EHDA at -2500 V

Aim 2: Identify the parameters suitable to achieve stable, surfactant free synthesis via LLE.

Experiments were done to identify the best combination of the flow rate and the applied voltage that consistently generate a cloud. It is noted that it is difficult to discern the spraying mode at

different operating conditions, unless a high speed camera is used. However, the desired emulsion droplets were always observed at the maximum flow rate and voltage allowed for the syringe pump and the high voltage power supply being used, respectively. Chloroform was delivered at a constant flow rate of 12.7 ml/h. High voltage was applied at the top of the needle using a high voltage power supply. It was found that a washing step in between each experimental trial is required, including thorough washing not only of the glass vial and the needle, but also of the ceramic insulator. In fact, the ceramic insulator needs to be clean to properly disperse the organic liquid. The most effective method identified was isopropanol washing, followed by drying using either air or nitrogen. Figure 8(B) shows the emulsification of chloroform using LLE; the voltage used was -2500 V. Instantaneous cloud formation was observed without the addition of surfactant. Thus, the dispersed phase was emulsified in ultrapure water (10m ml). The collection dish was placed on a rocker for 2.5 h to promote self-assembly via IS.

The absence of a surfactant in the continuous phase is a significant difference between LLE and Aero-IS. In Aero-IS, the emitted droplets are exposed to air before the collection in the aqueous medium. The aqueous droplet surrounding the volatile organic droplet not only helps stabilizing the droplet form, but also prevent unwanted evaporation of organic droplets in the air. In addition, fluid ejecting from the needle experiences body forces and both normal and tangential stresses at the interface between the fluid and the continuous phase (i.e. air). In order to achieve a stable spray in cone-jet mode, the surface tension of moving fluid needs to be reduced. Hence, the aqueous phase (i.e. PVA solution) is supplemented with surfactant that helps spraying fine emulsion droplets in the converged jet. In LLE, adding a surfactant in the aqueous phase was found to have a significant effect on dispersion. EHDA via LLE using 5% w/v PVA resulted in significantly higher conductivity of the aqueous phase; as a result, the electric field could not be established

because the equipotential state was reached in the continuous phase. The effect of PVA surfactant on EHDA inevitably made the synthesis process PVA free. The configuration developed is one of the few emulsion-based synthesis methods in a surfactant free environment. which provides great advantage by removing the downstream purification process and reducing the toxicity of products being used for biological applications.

Aim 3: Evaluate the uniformity and functionality of nanocomposites synthesized via LLE.

Nanocomposites of interest include empty micelles, SuperMags, and MultiDots. Initial studies revealed that the proposed LLE configuration is capable of dispersing chloroform in ultrapure water. PS-PEO is very soluble in chloroform. Therefore, we attempted to disperse PS-PEO solubilized in chloroform at the same operating conditions mentioned in the previous section, and found that they are suitable for EHDA of BCP solution. In addition to BCP, QDs and SPIONs are also soluble in chloroform. NPs solubilized in chloroform also showed a successfully emulsification via LLE with the same operating conditions. Table 1 summarizes the organic phase constituents, concentration, volume, and R (molar ratio of NP to Polymer) processed for each of nanocomposites.

Table 1. Organic phase constituents, concentration, volume, and R processed via LLE.

	PS-PEO (10 mg/ml)	QDs (3.5 mg/ml)	SPIONs (2.5 mg/ml)	$CHCl_3$	R
	volume used (µl)				
Empty Micelles	100	-	-	100	-
SuperMags	100	-	20	180	0.01
MultiDots	100	100	-	100	0.006

Micelle Characterization

Micelle characterization was first done using transmission electron microscopy (TEM). Ted Pella Inc TEM grids were cleaned using a PELCO easiGlowTM Glow Discharge Cleaning System. Then, 12.5 μL of sample was pipetted onto a silicone pad and the grid was placed over the sample

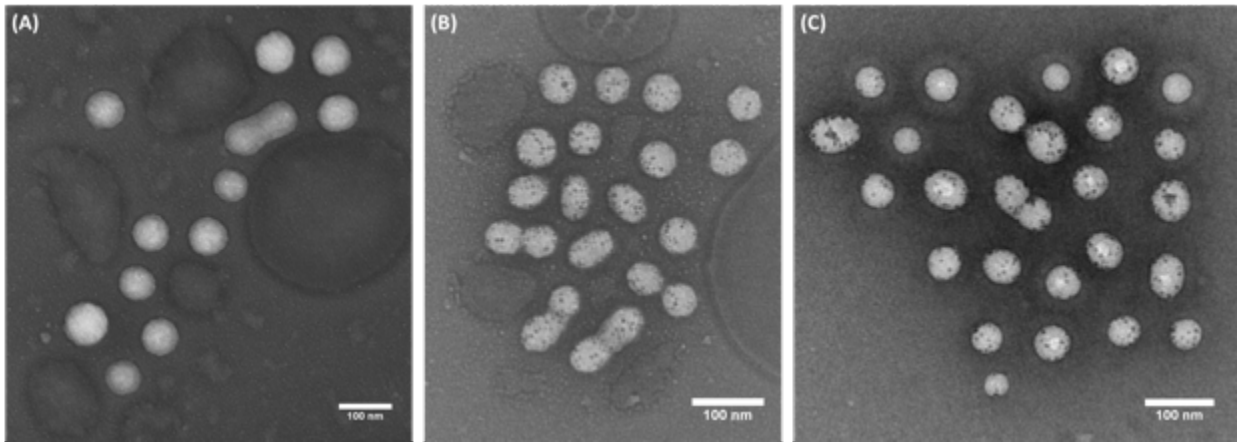

Figure 10. TEM images of (**A**) empty micelles, (**B**) SuperMags, and (**C**) MultiDots

droplet with the support film facing the droplet surface. Micelles were loaded on the grid for 5 min, then the excess liquid was slowly removed using filter paper. Negative staining was performed by placing the micelle loaded grid over 12.5 μL of a 1% uranyl acetate droplet for 5 min. The excess uranyl acetate was slowly removed using filter paper. The grid was imaged using an FEI Tecnai G2 Biotwin TEM.

Figure 9 shows TEM images of empty micelles, SuperMags and Multidots synthesized using LLE; the encapsulation of NPs is clearly visible. ImageJ analysis was performed on the images to further characterize the nanocomposites. Feret length, the longest distance from one end to the other in an object, was used as a characteristic length of the nanocomposites. Morphology can be categorized by the aspect ratio (AR) of a geometric shape. The AR is defined as the ratio of the length scales in different dimensions of an object. Each nanocomposite was categorized as either a sphere (AR 1 to 1.3), ellipse (AR 1.3 to 2), or worm (AR 2 or higher) based on its AR. Three samples of empty micelles, SuperMags, and MultiDots were synthesized via LLE. After analyzing individual

nanocomposites, the results were analyzed to obtain following information: (1) percent distribution of nanocomposites between different morphologies, (2) most frequently found range of Feret length (L_F), (3) geometric variance of each morphology by the aspect ratio (σ_{AR}) for nanocomposites of different morphology, (4) size distribution normalized by the number of most frequently found Feret length, and (5) Gaussian, or normality of size distributions.

Table 2. TEM image analysis for empty micelles, SuperMags (R = 0.01), and MultiDots (R = 0.006)

Empty Micelles	**% by N**	**L_F (nm)**	**σ_{AR}**	**Mode (nm)**
Sphere	86 ± 3.18	72.21 ± 5.53	1.08 ± 0.013	70 – 80
Ellipse	9 ± 1.52	109.02 ± 5.85	1.71 ± 0.043	110 – 120
Worm	5 ± 1.68	135.34 ± 12.47	2.26 ± 0.024	130 – 140
SuperMags	**% by N**	**L_F (nm)**	**σ_{AR}**	**Mode (nm)**
NP to BCP molar ratio (R) = 0.01				
Sphere	74 ± 3.73	64.23 ± 7.06	1.08 ± 0.0035	55 – 65
Ellipse	15 ± 2.44	88.67 ± 13.34	1.64 ± 0.013	85 – 95
Worm	11 ± 5.43	121.09 ± 17.29	2.42 ± 0.15	115 – 125
MultiDots	**% by N**	**L_F (nm)**	**σ_{AR}**	**Mode (nm)**
NP to BCP molar ratio (R) = 0.006				
Sphere	88 ± 1.11	51.79 ± 6.39	1.09 ± 0.01	45 – 55
Ellipse	9 ± 1.18	70.48 ± 9.34	1.52 ± 0.24	60 – 70
Worm	3 ± 0.11	95.76 ± 8.98	2.36 ± 0.03	80 – 90

Table 2 summarizes the results obtained from ImageJ analysis for empty micelles, SuperMags, and MultiDots. This data establish the reproducibility of nanocomposite synthesis via LLE. Although the cloud formation may appear slightly different between trials (the cloud forming spray

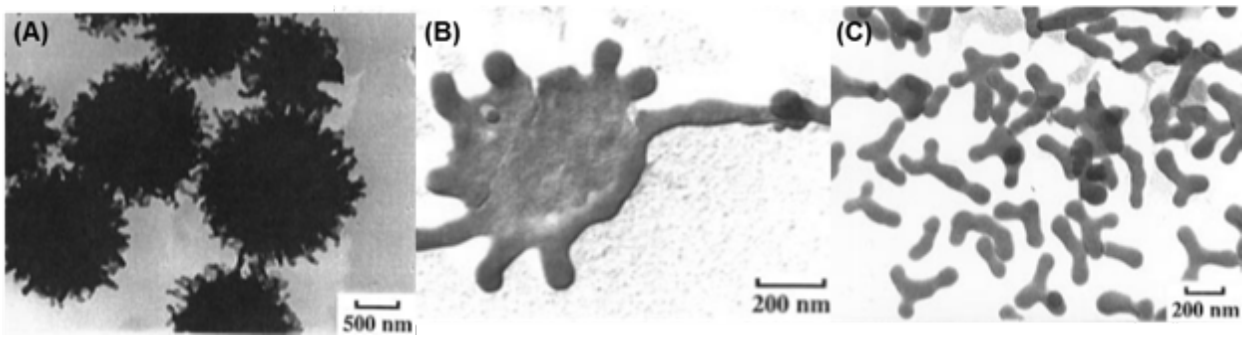

Figure 11. TEM images of various micelle morphology: (**A**) PS(240)-b-PEO(80) Large sphere with protruding rods (LCRM), (**B**) PS(240)-b-PEO(45): lamellae, and (**C**) PS(240)-b-PEO(15): branched short rods.[46]

might be pulsing), as long as the dispersion is not disturbed to the extent that the emulsion droplets aggregate, the uniformity of final products was well preserved.

In general, the most frequently found morphologies of micelles include spheres, rod-like, lamellae, and vesicles in dilute solution.[46-49] Spheres are the most predominant morphology of the micelles,

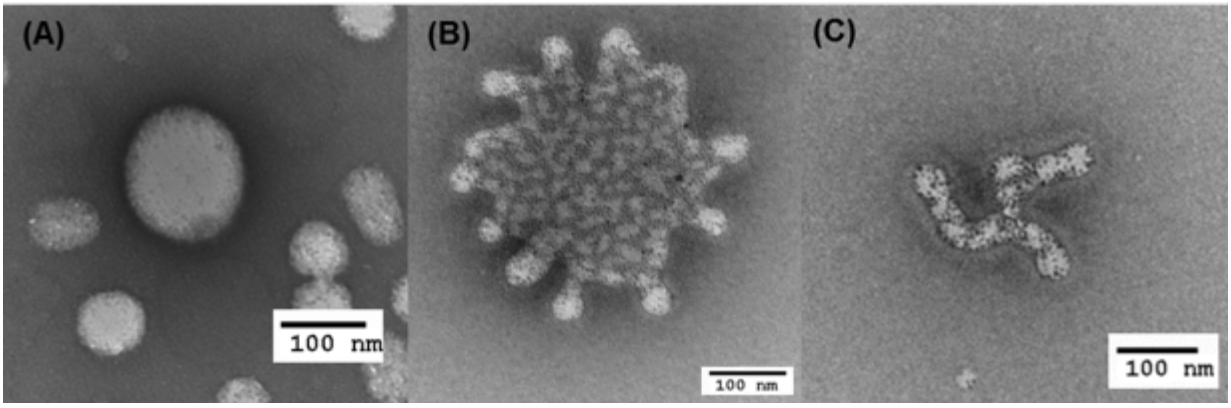

Figure 12. TEM images of SuperMags with high SPIONs concentration (R ~ 0.05): (**A**) large compound micelle (LCM), (**B**) lamellae encapsulating SPIONs, and a (**C**) branched short rod

which suggests the spherical geometry of core-shell, hydrophobic-hydrophilic, is the most favorable structure. Rod-like micelles have cylindrical, or tubular, geometry.

In this study, worm micelles fall into this category. Ellipse is a more arbitrary category that is neither a sphere, nor truly rod-like. Two important observations were made from the data. First, all three types of nanocomposites synthesized had predominantly spherical morphology, which agrees with the typical BCP aggregates formed via solution approaches. Second, the distributions of morphologies shift toward non-spherical micelles for NPs encapsulating micelles when NPs to BCP ratio increases. For example, the morphology distributions for empty micelles and MultiDots (R = 0.006) were very similar. However, the morphology distributions for SuperMags (R = 0.01), which had higher NP to BCP ratio, and empty micelles (and MultiDots) were significantly different: SuperMags had approximately 77 percent compared to 84 percent for empty micelles. The Eisenberg group illustrated the factors that lead to various morphologies of amphiphilic BCP in dilute solution. In a series of papers studying micelle morphologies, the Eisenberg group demonstrated the effect of the hydrophilic portion of BCP chain length. Studies suggest that decreasing the length of the PEO segment of the BCP results in the transition from sphere to rod-like morphology.[46]

The Eisenberg results may help explain the increase in the number of ellipses and worms for SuperMags and MultiDots relative to empty micelles. The presence of hydrophobic NPs effectively mimics the increased hydrophobic segment, or decreased hydrophilic segment. As a consequence, NPs encapsulating composites assemble to form more ellipses and worms. This phenomenon can be further explained by NPs encapsulating composites assembled at higher NP concentration. Figure 12 shows SuperMags synthesized via LLE at NPs to BCP molar ratios of approximately 0.05, which is 5 times higher than SuperMags characterized in Table 2. It was noted that the dominant morphology in the case of R = 0.05 was rod-like. Although not quantified, the

number frequencies of the morphologies shown in Figure 12 were high enough to be easily found on a TEM grid.

NPs arranged in large micelles and, especially, in lamellae displayed a patterned alignment, which suggests the phase separation of BCP chains inside of micelle. BCP arrangement that can illustrate this phenomenon is also suggested by the Eisenberg group in that the aggregates of reverse micelles, as shown in Figure 13., with a hydrophilic corona can occur as the PEO block is shortened, or if ions (i.e. $CaCl_2$, NaCl) are present at micro to milli molar concentrations.[47,50]

Third, the data also suggested that composites encapsulating NPs are smaller than empty micelles. Although it is not clear why SuperMags and MultiDots are significantly smaller than empty micelles, a hypothesis was put forward for further investigation. First, the increased NPs concentration might increase the driving force for BCP to produce more micelles in response to the presence of more hydrophobic NPs. Hence, given a fixed number of BCP chains, the effort to make more micelles can result in small nanocomposites comprised with fewer BCP chains per micelle. Second, the affinity between the NPs' surface ligand and PS might cause the self-assembly of micelles to be more, or less, favorable. Although how the ligand affinity to the PS segment affects the self-assembly process is not clear at this point, it is speculated that the degree of attraction/repulsion might influence how the BCP chain packs and orients in forming the micelles. Third, the formation of aggregates via a kinetically driven mechanism cannot be ruled out completed. Although LLE is based on the emulsification of organic solvents undergoing IS, for the LLE, this is fairly rapid. In fact, the total running time at current

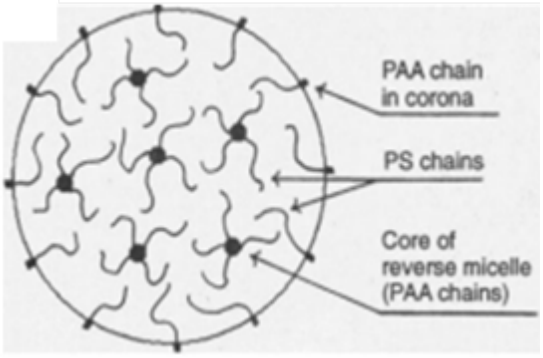

Figure 13. Schematic of large aggregates with reverse micelles at the core.[47]

operating condition for emulsification is roughly 57 seconds for 0.2 ml organic solution. In addition, $CHCl_3$ evaporation is observed to be faster for emulsions made via LLE in comparison to other process (i.e. sonication). Quantifiable measurement of the speed at which the cloudy emulsion droplets vanishes have not been made. However, the cloudy oil/water solution becomes transparent within the first several minutes on a rocker versus approximately 30 minute to 1 hour in the case of emulsion droplets formed via probe sonication. Based on this observation, it is possible that the thermodynamically driven IS process may be experiencing kinetically driven aggregation/nucleation. These hypotheses will be tested and validated in the future.

In order to test the functionality of nanocomposites, MultiDots were chosen as a model nanocomposite. The fluorescence intensity and stability were measured using a fluorometer. Table 3 shows the fluorescent counts measured for three MultiDots samples over the first 24 hour timespan after the synthesis.

Table 3. Fluorescent decay measurements of MultiDots

	Fluorescent count (1/s)		
Sample I.D.	0 h	24 h	I/Io
1	35415.78	1167.36	0.03
2	36355.28	2354.47	0.06
3	37050.51	1793.85	0.05

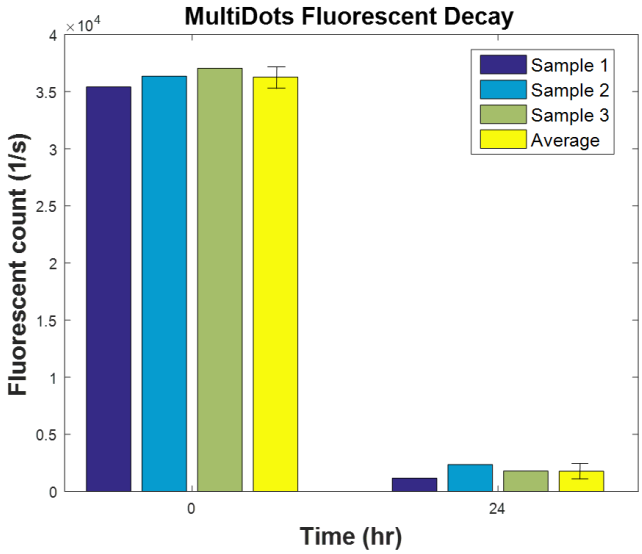

Figure 14. Rapid fluorescent decay observed within the first 24 hours for MultiDots synthesized via LLE

Rapid fluorescent decay was observed for the majority of MultiDots synthesized via LLE. It was noted that the quality of QDs varies depending on the vendor that makes the fluorescent NPs. In addition, batch-to-batch variation in terms of the stability was frequently observed regardless of which vendor QDs were purchased from. Given this inevitable instability of QDs from the user's perspective, the fluorescent decay rates were significantly higher for MultiDots prepared via LLE in comparison to those prepared via sonication methods. It is believed that the rapid decay of fluorescent may result from the absence of surfactant in the aqueous phase.

The role of surfactant in oil/water emulsification is known to stabilize the emulsion droplets in the immiscible continuous phase. In the case of Aero-IS, the surfactant is required to lower the surface tension of dispersed phase to allow the deformation of spray mode to cone-jet. To our best knowledge, the effect of surfactant on the stability of assembled nanocomposites has not been explored vigorously. In our group, additional studies are being performed to explore the role of surfactants on MultiDot functionality. Studies include the use of different types of surfactants to synthesize MultiDots using bath sonication. The same experiments and analysis will be conducted for MultiDots produced via LLE. While investigating the effect of surfactant on the functionality of MultiDots, the effort to enhance fluorescence duration needs to be made. In order to accomplish this goal, two experimental procedures are being considered. First, in order to minimize the

oxidation of quantum dot surface, the synthesis can be done under an oxygen free, and other impurity free, environment. Although it is challenging to completely remove oxygen, a number of modifications suitable to remove as much oxygen as possible can be done. Chloroform can be dried using molecular sieves, which will remove trace quantities of ethanol and water molecules. Also, argon sparging can be used in a closed vial that holds and collects the aqueous phase. Third, the IS process can occur in an argon environment. Second, in order to prevent undesired molecules (i.e. water) from entering the corona, the opportunity to cross-link the hydrophilic corona will be explored. The Wooley group reported crosslinking of a PAA shell in core-shell PS-PAA micelles to generate shell-cross-linked macromolecular structures (SCK's).[51] Kang et al. also utilized crosslinking of the shell to encapsulate gold NPs, shown in Figure 15.[52] It is expected that by crosslinking the corona, the enclosed QDs will be better protected from small impurities in aqueous phase, including the water molecules.

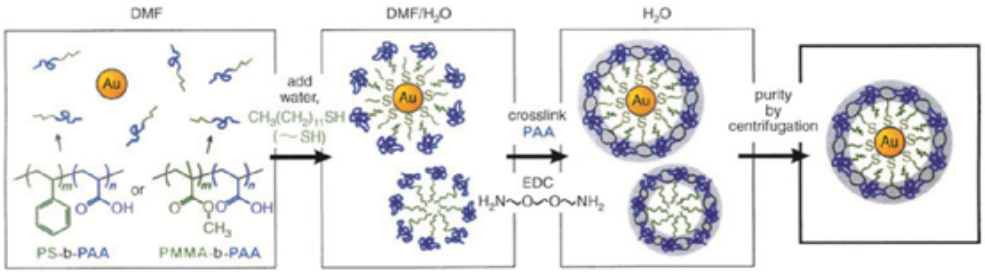

Figure 15. Schematic of crosslinking hydrophilic corona of micelles.[52]

Aim 4: Develop the next generation micellar electrospray configuration using a membrane filter to further optimize the process.

The proposed work is expected to demonstrate a semi-continuous, therefore higher throughput, synthesis route that is surfactant free. In **Aim 4**, the opportunity to incorporate a membrane filter to further scale-up the electrospray configuration will be explored. Sato et al. suggested that liquid-liquid atomization via a membrane filter can be achieved. Their alternative configuration replaced

the singe nozzle with membrane filters of different properties as listed in Table 4. This study reported that the same cloud formation occurred, and the average droplet sizes were almost the same, claiming the minimal difference in atomization and final products (water glass silica particle in micron size) between different membrane types. In addition, the throughput by volume was increased by more than 50 times compared to the single nozzle atomization platform.[53]

Table 4. Membrane filter types/properties for liquid-liquid atomization shown by Sato et al.[53]

Properties	Mixed Cellulose Ester	Hydrophilic PTFE	Polycarbonate
Pore Diameter (um)	0.45	0.45	0.4
Porosity	79	80	20
Thickness (um)	150	35	10

Modified LLE Configuration

An alternative LLE configuration is proposed based on the study mentioned above. Figure 16. shows the schematic of the next generation of LLE in which a membrane filter is supported at the bottom of the organic reservoir. Although not specifically defined, the organic reservoir needs to have a metallic portion so that high voltage can be applied. In addition, the portion of the reservoir that the membrane filter is attached to needs to be insulated using either ceramic or glass tube/ring. Preliminary studies were performed using two modified LLE configurations. Figure 17(A) shows the current LLE nozzle set up with a PTFE membrane attached at the bottom. Here, attaching the small PTFE membrane filter at the bottom of the 27 gauge nozzle was challenging. Therefore, a larger ~ 20 gauge needle was used. Figure 17(C) shows the PTFE membrane filter attached at the bottom of a $CHCl_3$ resistant chemical vial cap with a 27 gauge nozzle. Emulsification using both configurations failed for a variety of reasons. First, the adhesive used to attach the membrane filter

was not sufficiently adhesive and a leak occurred. A single trial using Figure 17(A) had the membrane filter attached for some time before it leaked. During the time the filter was still properly in place, a semi-cloudy dispersion was observed. A more refined membrane-incorporated LLE configuration is being developed, and it is expected that the nanocomposite synthesis via LLE can be accomplished at even higher throughput in the future.

Conclusion and Future Plans

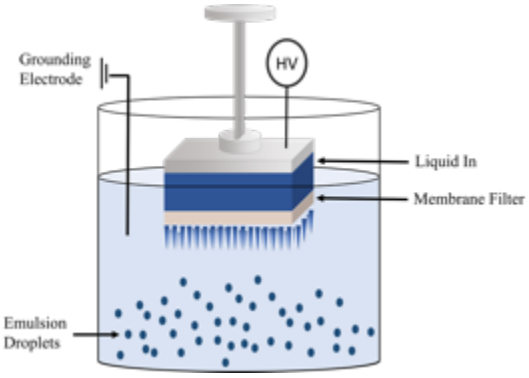

Figure 16. Schematic of alternative LLE configuration incorporating a membrane filter.

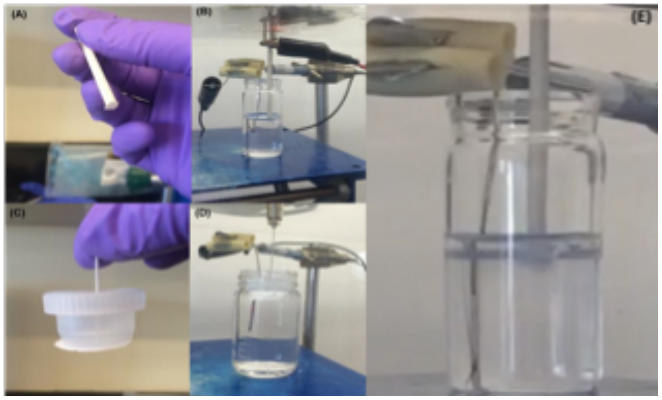

Figure 17. Membrane filer attached modified LLE configuration (**A**) PTFE attached at the bottom of single nozzle, (**B**) LLE set up using (A), (**C**) PTFE attached at the bottom of $CHCl_3$ resistant cap, (**D**) LLE set up using (C), and (**E**) semi-cloudy dispersion using (A).

LLE is a nanocomposite synthesis route that demonstrates stable emulsification and self-assembly of micelles in a surfactant free environment. To date, operating conditions suitable for producing empty micelles, SuperMags, and MultiDots have been identified, and product uniformity has been confirmed. In comparison to other laboratory scale synthesis routes, LLE is faster and more tunable. The model nanocomposites used to test functionality of products were MultiDots, which exhibit fluorescent signals from the QDs. Studies showed that fluorescence decay was more rapid than that of comparable products prepared via the sonication method. Other than the method of emulsifying the organic solvent, the main difference between sonication and LLE methods was the use of surfactant. It is suspected that the presence of surfactants (i.e. PVA) helps stabilize micelles to protect and preserve the functionality of NPs at the core of the micelles; although the

core region of micelle is hydrophobic, it is possible for small molecules (i.e. water, oxygen) to pass through the hydrophilic corona and cause NPs to lose fluorescence. There are additional sub-Aims proposed based on the results presented in this report include:

1. Identify the factors that cause the rapid fluorescent decay and improve nanocomposite functionality
    - Preparation and synthesis under Argon rich environment
    - Cross-linking hydrophilic corona
    - Studying the role of surfactants on the functionality
2. Utilize MultiDots made via LLE to label cancer cells for bio-imaging
3. Develop a membrane filter incorporated LLE configuration for higher throughput

References

1. Park, J.-H., et al. (2008). "Micellar hybrid nanoparticles for simultaneous magnetofluorescent imaging and drug delivery." Angewandte Chemie-International Edition **47**(38): 7284-7288.

2. Insin, N., et al. (2008). "Incorporation of iron oxide nanoplarticles and quantum dots into silica microspheres." Acs Nano **2**(2): 197-202.

3. Yi, D. K., et al. (2005). "Silica-coated nanocomposites of magnetic nanoparticles and quantum dots." Journal of the American Chemical Society **127**(14): 4990-4991.

4. Deng, S., et al. (2010). "Interactions in fluorescent-magnetic heterodimer nanocomposites." Nanotechnology **21**(14).

5. Ruan, G., et al. (2010). "Simultaneous Magnetic Manipulation and Fluorescent Tracking of Multiple Individual Hybrid Nanostructures." Nano Letters **10**(6): 2220-2224.

6. Ruan, G. and J. O. Winter (2011). "Alternating-Color Quantum Dot Nanocomposites for Particle Tracking." Nano Letters **11**(3): 941-945.

7. Thakur, D., et al. (2009). "pH sensitive CdS-iron oxide fluorescent-magnetic nanocomposites." Nanotechnology **20**(48).

8. Corr, S. A., et al. (2008). "Multifunctional magnetic-fluorescent nanocomposites for biomedical applications." Nanoscale Research Letters **3**(3): 87-104.

9. Riess, G. (2003). "Micellization of block copolymers." Progress in Polymer Science **28**(7): 1107-1170.

10. Zhu, J. and R. C. Hayward (2008). "Spontaneous generation of amphiphilic block copolymer micelles with multiple morphologies through interfacial instabilities." Journal of the American Chemical Society **130**(23): 7496-7502.

11. Duong, A. D., et al. (2014). "Scalable, Semicontinuous Production of Micelles Encapsulating Nanoparticles via Electrospray." Langmuir **30**(14): 3939-3948.

12. Letchford, K. and H. Burt (2007). "A review of the formation and classification of amphiphilic block copolymer nanoparticulate structures: micelles, nanospheres, nanocapsules and polymersomes." European Journal of Pharmaceutics and Biopharmaceutics **65**(3): 259-269.

13. Bakalova, R., et al. (2006). "Silica-shelled single quantum dot micelles as imaging probes with dual or multimodality." Analytical Chemistry **78**(16): 5925-5932.

14. Kircher, M. F., et al. (2003). "A multimodal nanoparticle for preoperative magnetic resonance imaging and intraoperative optical brain tumor delineation." Cancer Research **63**(23): 8122-8125.

15. Mulder, W. J. M., et al. (2007). "Magnetic and fluorescent nanoparticles for multimodality imaging." Nanomedicine **2**(3): 307-324.

16. Prasad, P. N. (2006). "Emerging opportunities at the interface of photonics, nanotechnology and biotechnology." Molecular Crystals and Liquid Crystals **446**: 1-10.

17. Sharma, P., et al. (2006). "Nanoparticles for bioimaging." Advances in Colloid and Interface Science **123**: 471-485.

18. Wang, S., et al. (2007). "Core/shell quantum dots with high relaxivity and photoluminescence for multimodality imaging." Journal of the American Chemical Society **129**(13): 3848-3856.

19. Dubertret, B., et al. (2002). "In vivo imaging of quantum dots encapsulated in phospholipid micelles." Science **298**(5599): 1759-1762.

20. Gao, X. H., et al. (2004). "In vivo cancer targeting and imaging with semiconductor quantum dots." Nature Biotechnology **22**(8): 969-976.

21. Han, M. Y., et al. (2001). "Quantum-dot-tagged microbeads for multiplexed optical coding of biomolecules." Nature Biotechnology **19**(7): 631-635.

22. Salgueirino-Maceira, V., et al. (2006). "Composite silica spheres with magnetic and luminescent functionalities." Advanced Functional Materials **16**(4): 509-514.

23. Song, C. X., et al. (1997). "Formulation and characterization of biodegradable nanoparticles for intravascular local drug delivery." Journal of Controlled Release **43**(2-3): 197-212.

24. Dorcena, C. J., et al. (2013). "Characterization and toxicity of carbon dot-poly (lactic-co-glycolic acid) nanocomposites for biomedical imaging." Nano Life **3**(01): 1340002.

25. Bae, J., et al. (2012). "Multifunctional Nanoparticle-Loaded Spherical and Wormlike Micelles Formed by Interfacial Instabilities." Advanced Materials **24**(20): 2735-2741.

26. Granek, R., et al. (1993). "Dynamics of spontaneous emulsification." Journal de Physique II **3**(6): 829-849.

27. Johnson, B. K. and R. K. Prud'homme (2003). "Flash nanoprecipitation of organic actives and block copolymers using a confined impinging jets mixer." Australian Journal of Chemistry **56**(10): 1021-1024.

28. Gindy, M. E., et al. (2008). "Composite block copolymer stabilized nanoparticles: simultaneous encapsulation of organic actives and inorganic nanostructures." Langmuir **24**(1): 83-90.

29. Cheng, J. C., et al. (2010). "A competitive aggregation model for flash nanoprecipitation." Journal of Colloid and Interface Science **351**(2): 330-342.

30. Shen, H., et al. (2011). "Self-assembling process of flash nanoprecipitation in a multi-inlet vortex mixer to produce drug-loaded polymeric nanoparticles." Journal of Nanoparticle Research **13**(9): 4109-4120.

31. Valente, I., et al. (2012). "Nanoprecipitation in confined impinging jets mixers: Production, characterization and scale-up of pegylated nanospheres and nanocapsules for pharmaceutical use." Chemical engineering science **77**: 217-227.

32. Melcher, J. and G. Taylor (1969). "Electrohydrodynamics: a review of the role of interfacial shear stresses." Annual Review of Fluid Mechanics **1**(1): 111-146.

33. Zeleny, J. (1917). "Instability of electrified liquid surfaces." Physical review **10**(1): 1.

34. Taylor, G. (1964). Disintegration of water drops in an electric field. Proceedings of the Royal Society of London A: Mathematical, Physical and Engineering Sciences, The Royal Society.

35. Jaworek, A. and A. Krupa (1998). Main modes of electrohydrodynamic spraying of liquids. Third International Conference on Multiphase Flow, Lyon, France. Retrieved from: http://www/. imp. gda. pl/fileadmin/old_imp/ehd/lyon-98s. pdf.

36. Loscertales, I. G., et al. (2002). "Micro/nano encapsulation via electrified coaxial liquid jets." Science **295**(5560): 1695-1698.

37. Wu, Y., et al. (2010). "Coaxial electrohydrodynamic spraying of plasmid DNA/polyethylenimine (PEI) polyplexes for enhanced nonviral gene delivery." Biotechnology and bioengineering **105**(4): 834-841.

38. Wu, Y., et al. (2009). "Coaxial electrohydrodynamic spraying: a novel one-step technique to prepare oligodeoxynucleotide encapsulated lipoplex nanoparticles." Molecular pharmaceutics **6**(5): 1371-1379.

39. SmartMeasurement/ "Conductivity" http://www.smartmeasurement.com/calculators-utilities/conductivity

40. Sato, M., et al. (1993). "Emulsification and size control of insulating and/or viscous liquids in liquid-liquid systems by electrostatic dispersion." Journal of Colloid and Interface Science **156**(2): 504-507.

41. Barrero, A., et al. (2004). "Steady cone-jet electrosprays in liquid insulator baths." Journal of Colloid and Interface Science **272**(1): 104-108.

42. Yeh, C. H., et al. (2012). "Using an electro-spraying microfluidic chip to produce uniform emulsions under a direct-current electric field." Microfluidics and Nanofluidics **12**(1-4): 475-484.

43. Tsouris, C., et al. (1994). "Electrostatic spraying of nonconductive fluids into conductive fluids." AIChE journal **40**(11): 1920-1923.

44. Sato, M., et al. (2009). "Production of Nano-silica Particles in Liquid-liquid System by Pulsed Voltage Application." Ieee Transactions on Dielectrics and Electrical Insulation **16**(2): 320-324.

45. Sato, M., et al. (2009). "Dielectric Liquid-in-Liquid Dispersion by Applying Pulsed Voltage." Ieee Transactions on Dielectrics and Electrical Insulation **16**(2): 391-395.

46. Yu, K., et al. (1996). "Novel morphologies of "crew-cut" aggregates of amphiphilic diblock copolymers in dilute solution." Langmuir **12**(25): 5980-5984.

47. Zhang, L. F. and A. Eisenberg (1995). "MULTIPLE MORPHOLOGIES OF CREW-CUT AGGREGATES OF POLYSTYRENE-B-POLY(ACRYLIC ACID) BLOCK-COPOLYMERS." Science **268**(5218): 1728-1731.

48. Zhang, L. F. and A. Eisenberg (1996). "Morphogenic effect of added ions on crew-cut aggregates of polystyrene-b-poly(acrylic acid) block copolymers in solutions." Macromolecules **29**(27): 8805-8815.

49. Zhang, L. F. and A. Eisenberg (1996). "Multiple morphologies and characteristics of "crew-cut" micelle-like aggregates of polystyrene-b-poly(acrylic acid) diblock copolymers in aqueous solutions." Journal of the American Chemical Society **118**(13): 3168-3181.

50. Zhang, L., et al. (1996). "Ion-induced morphological changes in" crew-cut" aggregates of amphiphilic block copolymers." Science **272**(5269): 1777.

51. Huang, H., et al. (1997). "Hydrogel-coated glassy nanospheres: a novel method for the synthesis of shell cross-linked knedels." Journal of the American Chemical Society **119**(48): 11653-11659.

52. Kang, Y. and T. A. Taton (2005). "Core/shell gold nanoparticles by self-assembly and crosslinking of micellar, block-copolymer shells." Angewandte Chemie **117**(3): 413-416.

53. Sato, M., et al. (2010). "Nozzleless EHD Spraying for Fine Droplet Production in Liquid-in-Liquid System." Ieee Transactions on Industry Applications **46**(6): 2190-2195.